Integrating Oxaliplatin with Highly Luminescent Carbon Dots: An Unprecedented Theranostic Agent for Personalized Medicine

Min Zheng, Shi Liu, Jing Li, Dan Qu, Haifeng Zhao, Xingang Guan, Xiuli Hu, Zhigang Xie, Xiabin Jing, and Zaicheng Sun**

Theranostics, the combination of medical therapy and bioimaging diagnostics for optimizing the efficacy and safety of therapeutic regimes, is a growing field that is paving the way towards the goal of personalized medicine for the benefit of patients.[1–4] Emerging nanotechnology has offered great opportunities to design and generate such nanoparticle-based theranostic agents.[3,4] If we consider the different types of nanoparticles, theranostic agents include those based on iron oxide,[4,5] quantum dots (QDs),[6] gold nanoparticles,[7] carbon nanoparticles,[2,8] and silica nanoparticles.[9] Within the last decade, various theranostic agents have been developed by combination of many kinds of therapy techniques, for example, chemotherapy, radiation therapy, and photo-triggered therapy, with various imaging techniques, such as magnetic resonance imaging (MRI) and ultrasonic, radiological, and optical imaging. Compared with other imaging techniques, optical imaging has numerous advantages, for example, high contrast, high sensitivity, and controllable targeting.[10] Recently, optical imaging technology has undergone explosive development with the emergence of light-emitting nanocrystals, which have a tiny size (a few to tens of nanometers), tunable color, and high photoluminescence quantum yield (PL QY).[11] However, QD-based theranostic agents are relatively limited due to the innate toxicity of QDs. This problem is most prominent in first-generation QDs, where toxic Cd and Pb are employed in the preparation. There is great interest in synthesizing non-toxic, highly luminescent QDs.[3]

Fluorescent carbon dots (CDs) have attracted a great deal of attention owing to their unique properties, such as high solubility in water, flexibility in surface modification, nontoxicity, excitation-dependent multicolor emission, excellent biocompatibility, good cell permeability, and high photostability.[12] They can be easily obtained from graphite and organic molecules such as citric acid or glucose.[13] They have extensive potential applications in energy conversion, ion detection, and bioimaging fields.[13,14] Therefore, several groups have evaluated CDs as bioimaging agents, including their cellular uptake and fluorescence brightness in cellular or in vivo environments. However, few of them have been used as a theranostic agent.[2,15,16] It is possible for a CD to carry several therapeutic agents simultaneously on its surface by means of covalent bonding because a great many functional groups (such as amino, carboxyl, or hydroxyl) exist on the surface of carbon dots. Platinum-based drugs are very effective anticancer agents that are successfully used in nearly 50% of chemotherapeutic regimens administered to cancer patients.[17] Among platinum-based drugs, oxaliplatin is a relatively new platinum(II) complex that is currently being used in a new, promising pharmacotherapy of metastatic colorectal cancer.[18] However, its application is limited by its side effects and drug resistance. One approach to overcoming the drawbacks of Pt(II) complexes is to use Pt(IV) complexes (Oxa(IV)-COOH) as a prodrug, which can be easily obtained by addition of two axial ligands to a Pt(II) drug.[19] The carboxyl group of Oxa(IV)-COOH is able to conjugate with CDs to form a theranostic nanomedicine, which can be used to diagnose, carry out therapy, and monitor response to therapy.

Here, we report a brand new theranostic nanomedicine (CD-Oxa) synthesized by means of the condensation reaction between the amino groups on the CD's surface and the carboxyl group of Oxa(IV)-COOH (**Scheme 1**). CD-Oxa integrates the optical properties of CDs and the anticancer function of oxaliplatin into a single unit. This nanomedicine possesses multiple functions: i) drug carrier: Oxa(IV)-COOH is attached to the CD's surface and the whole particle enters the cancer cells by endocytosis; ii) controlled drug release: the Oxa(IV)-COOH can be readily reduced to oxaliplatin(II) because of the intrinsic reducing environment in cancer cells; iii) multicolor imaging ability: the multicolor emission of CDs endows the CD-Oxa conjugate with bioimaging ability both in vitro and in vivo. By monitoring the fluorescence intensity of CD-Oxa, we can follow the track or distribution of the drug molecules. The in vivo results indicate that CD-Oxa has great potential applications in cancer diagnostics and therapy.

CDs were prepared by means of a modified thermal pyrolysis route, using citric acid (CA) as carbon source and polyene

Dr. M. Zheng, D. Qu, H. F. Zhao, Prof. Z. C. Sun
State Key Laboratory of Luminescence and Applications
Changchun Institute of Optics Fine Mechanics and Physics
Chinese Academy of Sciences
3888 East Nanhu Road, Changchun
Jilin 130033, P. R. China
E-mail: sunzc@ciomp.ac.cn

S. Liu, Dr. J. Li, Dr. X. G. Guan, Dr. X. L. Hu, Prof. Z. G. Xie, Prof. X. B. Jing
State Key Laboratory of Polymer Chemistry and Physics
Changchun Institute of Applied Chemistry
Chinese Academy of Sciences
5625 Renmin Street, Changchun, Jilin 130022, P. R. China
E-mail: xiez@ciac.ac.cn

S. Liu, D. Qu
University of Chinese Academy of Sciences
Beijing 100049, P. R. China

DOI: 10.1002/adma.201306192

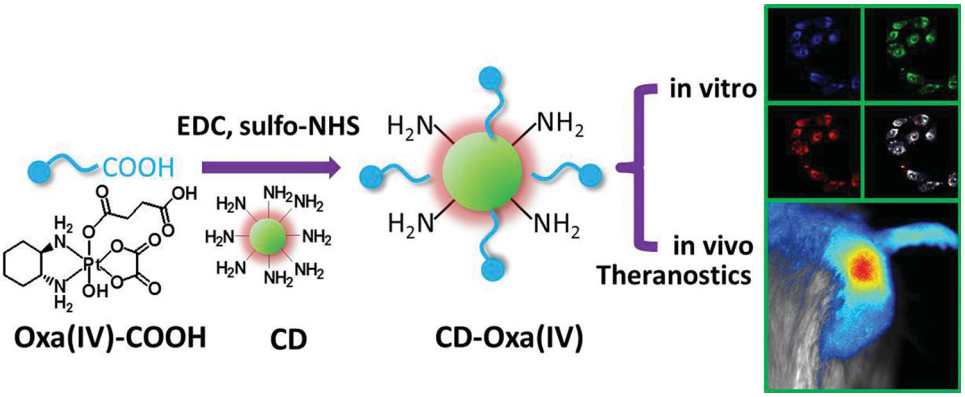

Scheme 1. Synthetic scheme for CD-Oxa and its applications in bioimaging and theranostics.

polyamine (PEPA) as passivation agent (see the experimental section in the Supporting Information).[20] Transmission electron microscopy (TEM) images reveal the uniform size (diameter = 2.28 ± 0.42 nm) of the CDs (**Figure 1**a). Well-resolved lattice fringes are observed in high-resolution TEM images, corresponding to *d* spacing values of 0.28 and 0.32 nm (Figure 1b–d), which are close to the values for the (020) and (002) planes of graphitic carbon, respectively,[16] indicating the graphitic nature of the CDs. Atomic force microscopy (AFM) images (Figure 1e) show that the as-prepared CDs disperse in the water and remain as individual particles. The height profile along a line discloses the height of CDs to range from 0.34 to 1.4 nm, corresponding to 1–4 layers of monolayer graphene sheets if the theoretical value of 0.34 nm is taken as the thickness of a single layer. CDs were characterized using X-ray photoelectron spectroscopy (XPS) in order to explore their elemental

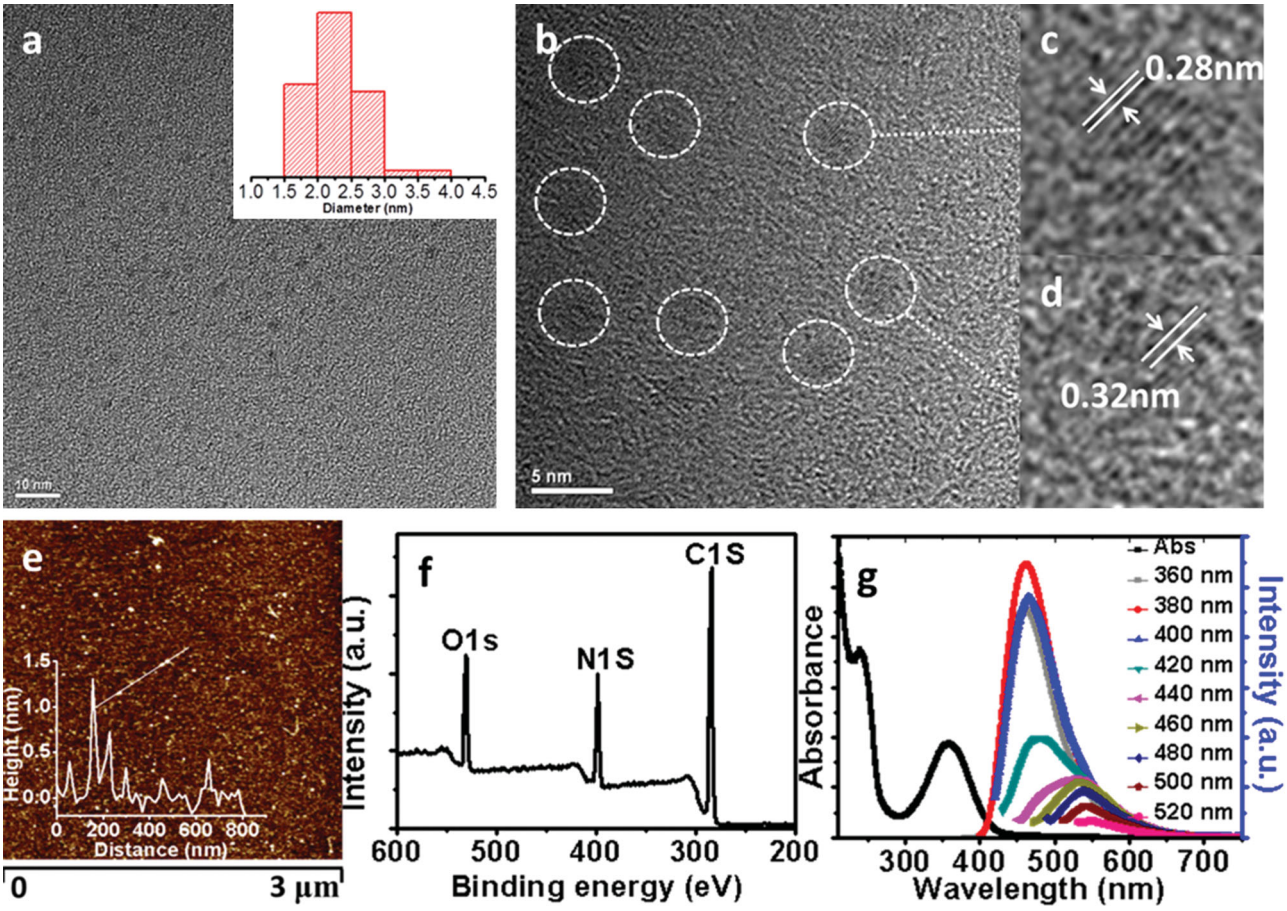

Figure 1. a) TEM image of CDs. Inset: Size distribution of CDs. b) HRTEM image of CDs. c,d) Typical single CD nanoparticles with lattice parameters of 0.28 nm and 0.32 nm, respectively. e) AFM image of CDs. Superimposed is the height profile along the line marked in the AFM image. f) XPS spectrum of the CDs. g) UV-vis absorption (black solid line) and photoluminescence spectra of CDs for different excitation wavelengths.

composition and chemical bonds. The full-scan XPS spectrum of CDs is shown in Figure 1f. Three peaks, at 284.0, 398.1, and 530.6 eV, are attributed to C 1s, N 1s, and O 1s, respectively. The ratio of N/O is 0.68, indicating that quite a fraction of N atoms are substitutionally doped into CDs. The high resolution XPS spectra of C 1s (Figure S2 in the Supporting Information) and N 1s (Figure S3) further confirm that C–C/C=C, C–N, C–O, C=O, and N–H bonds exist in CDs.[21] Fourier transform infrared (FTIR) spectra (Figure S4, Supporting Information) were used to identify the surface functional groups present on the CDs' surface. The broad absorption bands at 3000–3500 cm^{-1} are assigned to stretching vibrations of O–H and N–H, while the bands at 1557 and 1352 cm^{-1} originate from the bending vibrations of N–H and C–NH, respectively. That indicates that there are many amino groups on the surface of the CDs. These hydrophilic groups can help CDs disperse into aqueous solution and facilitate covalent conjugation with Oxa(IV)-COOH. The UV-vis absorption of CDs (Figure 1g) shows two clear bands at 240 and 360 nm, which are attributed to the π–π^* transition of the aromatic ring structure and n–π^* transition of C=O. As shown in Figure 1g, the as-obtained CDs exhibit typical excitation-dependent photoluminescent behavior, as previously reported.[12] With increasing excitation wavelength from 380 to 520 nm the emission peak redshifts from 462 to 550 nm. The maximum PL intensity was observed under excitation of 380 nm with the absolute QY of 21.0%. In other words, CDs can emit relatively bright green, orange, and red colors under the excitation of blue, green, and yellow light, respectively (Figure S5). The multicolor emission endows CDs with a great advantage over other labeling agents, because this gives us much freedom to choose a proper wavelength for optical imaging.

Before CDs were used for in vitro bioimaging, cellular biocompatibility experiments were carried out by MTT assay with L929 mouse fibroblast cells (L929) as the test cell line. As shown in Figure S6 (Supporting Information), the survival rates of L929 cells incubated with CDs at six different concentrations up to 0.5 mg mL^{-1} all exceed 75% relative to the control group cells without CD treatment, indicating that incorporation of CDs does not significantly influence the growth of cells. Therefore, CDs possess good biocompatibility and low toxicity, which makes them suitable for use as a bioimaging reagent.

To validate the multicolor property and imaging application of CDs, they were used as probes for confocal fluorescence imaging with a human hepatocellular liver carcinoma cell line (HepG2 cells). As seen in Figure S7 (Supporting Information), after incubation in culture medium to which CDs had been added, the cells displayed quite intense blue, green, and red colors upon excitation at 405, 488, and 555 nm, respectively. CDs were observed mainly in the cell membrane and the cytoplasm, especially around the cell nucleus. No blinking or photobleaching was observed in the laser scanning confocal microscopy (LSCM) study. The stabilities of the as-prepared CDs are also examined by long-time monitoring of fluorescent emission, which shows negligible changes of fluorescence intensity for 24 h under visible light illumination (Figure S8, Supporting Information). In short, given the multicolor property and remarkably high photostability, it is possible for CDs to act as an ideal bioimaging agent.

In order to integrate the therapeutic and bioimaging capabilities into one single agent, one derivative of oxaliplatin(IV) with a carboxyl group at its axial position was synthesized and named Oxa(IV)-COOH. The details of its synthesis and characterization have been described in a previous paper.[19] The carboxyl group of Oxa(IV)-COOH is activated by EDC/sulfo-NHS (ethyl(dimethylaminopropyl) carbodiimide/*N*-hydroxysuccinimide) and reacted with amino groups on CDs to form CD-Oxa (Scheme 1; the detailed procedure is described in the experimental section in the Supporting Information). In this nanomedicine, CDs act as the drug carrier and provide the bioimaging function, while Oxa(IV) contributes the anticancer capability; the aim is to monitor a treatment based on the imaging results, thereby providing more specific and efficient systems for advanced treatment of cancers.

The platinum content of CD-Oxa was determined by inductively coupled plasma mass spectrometry (ICP-MS) to be 1.5 wt%, corresponding to an Oxa(IV) content of 4.2 wt% in CD-Oxa. Measurements of zeta potential show that CDs have a positive surface potential of 24.02 mV; after conjugation, the zeta potential of CD-Oxa is 16.69 mV, which is slightly lower than that of CDs, also implying that only a small part of the positively charged amino groups of CDs were consumed during the conjugation of CDs with Oxa (IV)-COOH. The TEM image of CD-Oxa (**Figure 2**a) indicates uniformly dispersed CD-Oxa nanoparticles in aqueous media with narrow size distribution of 2.71 ± 0.43 nm, slightly larger than that of CDs (2.28 ± 0.42 nm, Figure 1a) as a result of the incorporation of Oxa(IV)-COOH. Well-resolved crystal lattices in high-resolution TEM (HRTEM) images (Figure 2b) are observed in CD-Oxa. Lattice spacings of 0.32 nm and 0.28 nm are observed in Figures 2c and 2d, which are the same as those of pristine CDs (Figures 1c and 1d). The AFM image illustrates the topographic morphology (Figure 2e), and the superimposed height distribution of the obtained CD-Oxa shows that the as-prepared CD-Oxa nanoparticles remain as individual particles. The height profile along the line in Figure 2e is mostly distributed in the range from 2.5 to 4.2 nm, which is greater than for CDs. This attributes to the modification of Oxa(IV)-COOH on the surface of CDs, resulting in the increase of diameters and heights.[22] XPS (Figures 1f,g, S9, S10) was also performed to determine the composition of CD-Oxa. The results (Figure 2f) indicate that CD-Oxa is mainly composed of C, N, and O atoms and the ratio of N/O is 0.56, which is less than that of the original CDs owing to the incorporation of Oxa(IV). In addition, a weak peak at 73.6 eV corresponding to Pt 4f is observed, further confirming successful synthesis of CD-Oxa. The high-resolution spectrum of Pt 4f (Figure 2g) shows two peaks, corresponding to Pt(IV) $4f_{7/2}$ (72.1 eV) and Pt(IV) $4f_{5/2}$ (75.2 eV), respectively. The FTIR spectrum (Figure S11, Supporting Information) of CD-Oxa is similar to that of CDs. The UV-vis and PL spectra of CD-Oxa are shown in Figure S12 (Supporting Information). The same absorption and PL emission bands as those of the original CDs are observed, indicating CD-Oxa also possesses excitation-dependent PL properties. The absolute QY of CD-Oxa is 19%, which is slightly lower than that of CDs. The high solubility of CD-Oxa in water (~270 mg mL^{-1}) enables it to be injected intravenously or intralesionally into the body of an animal.

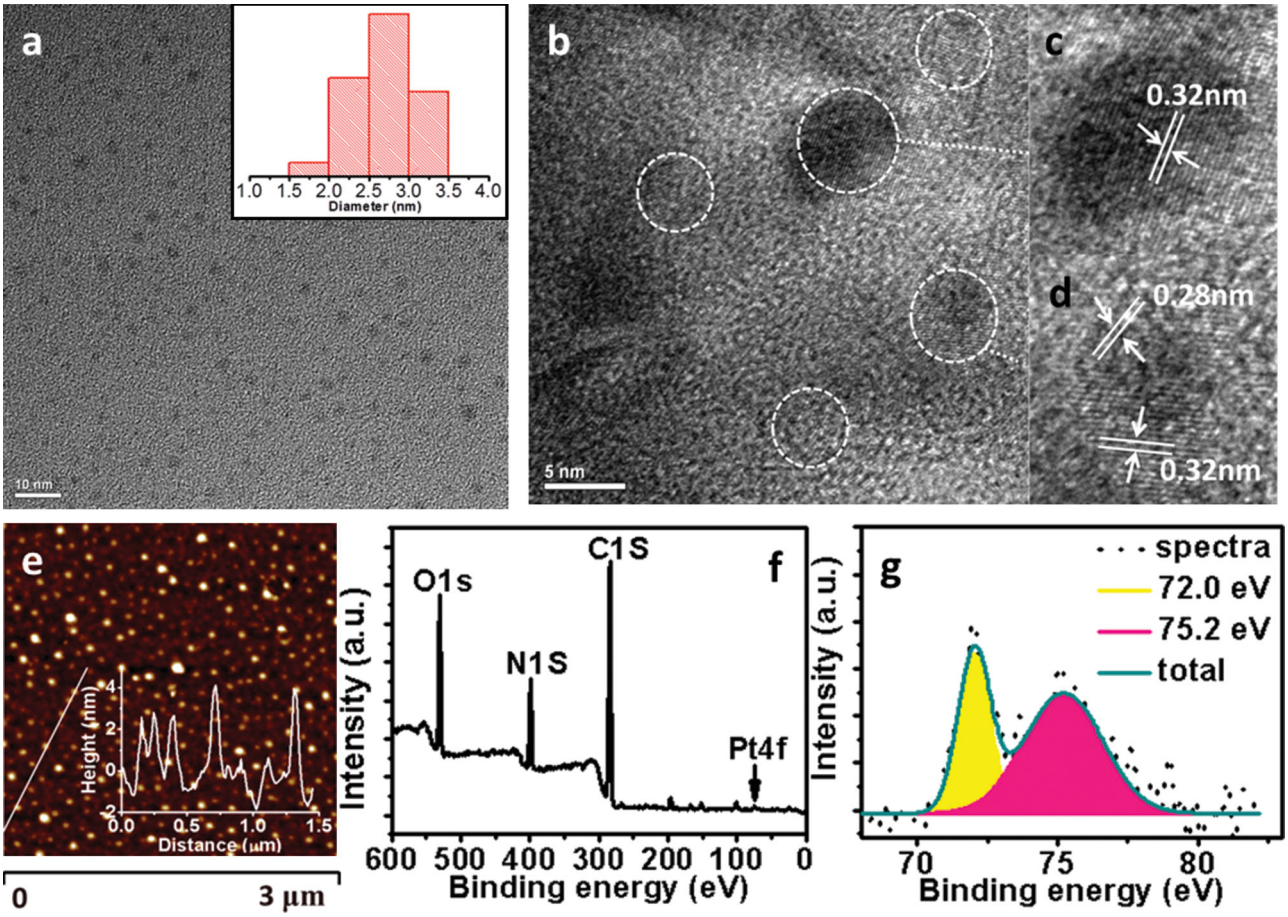

Figure 2. a) TEM image of CD-Oxa nanoparticles. Inset: Size distribution of CD-Oxa particles. b) HRTEM image of CD-Oxa nanoparticles. c,d) Typical single CD-Oxa nanoparticles with lattice parameters of 0.28 nm and 0.32 nm, respectively. e) AFM image of CD-Oxa. Superimposed is the height profile along the line marked in the AFM image. f,g) XPS spectrum (f) and high-resolution Pt 4f XPS spectrum (g) of CD-Oxa.

To prove that CD-Oxa can provide a high resolution for cell imaging, human epithelial carcinoma cells (HeLa cell line) were incubated with CD-Oxa for 1 h and then imaged with a confocal fluorescence microscope. As shown in **Figure 3**a–c, after incubation with CD-Oxa, the cells displayed quite intense blue, green, and red colors under laser excitation at wavelengths of 405, 488, and 555 nm, respectively. Most CD-Oxa was observed in the cell membrane and the cytoplasm, indicating that CD-Oxa particles had been internalized by the cells.

In vitro MTT assay was used to test the toxicities of oxaliplatin and CD-Oxa to HepG2 cells. HepG2 cells were exposed to either oxaliplatin or CD-Oxa in six doses (0.064 to 40 μg mL^{-1}) for 48 h. As shown in Figure 3f, for the HepG2 cell line, CD-Oxa is as cytotoxic as oxaliplatin(II) (IC_{50} = 3.4 μg mL^{-1}). According to our previous report, Oxa can be conjugated with different drug carriers.[19] These conjugated systems are very stable in the circulatory system and oxaliplatin could be released from the carrier–Pt(IV) conjugation under the intracellular reductive conditions.[19,23] CD-Oxa has release behavior similar to these Oxa conjugations. Therefore, the remarkable fluorescence and high cytotoxicity towards cancer cells endow CD-Oxa with an intrinsic capability of bioimaging and cancer therapy.

Intravenous chemotherapy often leads to severe complications and abandonment of therapy owing to systemic toxicity.[24] To overcome this problem, many recent studies have been devoted to alternative modes of delivery for anticancer drugs to decrease systemic toxicity and improve the therapeutic index for approved cancer drugs. Several studies have shown that intratumoral delivery of cytotoxic drugs by direct injection into the solid tumor mass can provide extremely high drug doses at the target site while minimizing systemic toxicity. Direct intratumoral chemotherapy therefore represents a new treatment paradigm that may be very valuable for treating cancers, especially when combined with imaging agents. In the present work, in order to control local disease and to avoid potential surgical complications and systemic toxicity, intralesional injection of CD-Oxa was used for the treatment of hepatocarcinoma 22 cell line (H22) liver cancer of Chinese Kun Ming (KM) mice. H22 xenograft models of hepatocarcinoma were established by injection of H22 cells into the lateral aspect of the anterior limb of KM mice. The mouse was injected with CD-Oxa (0.72 mg mL^{-1} of Pt, 20 μL) at the center of the tumor, and then imaged by a Maestro 500FL in vivo optical imaging system (Cambridge Research & Instrumentation, Inc.) under excitation with blue light (445–490 nm). The fluorescence signal of CD-Oxa can also

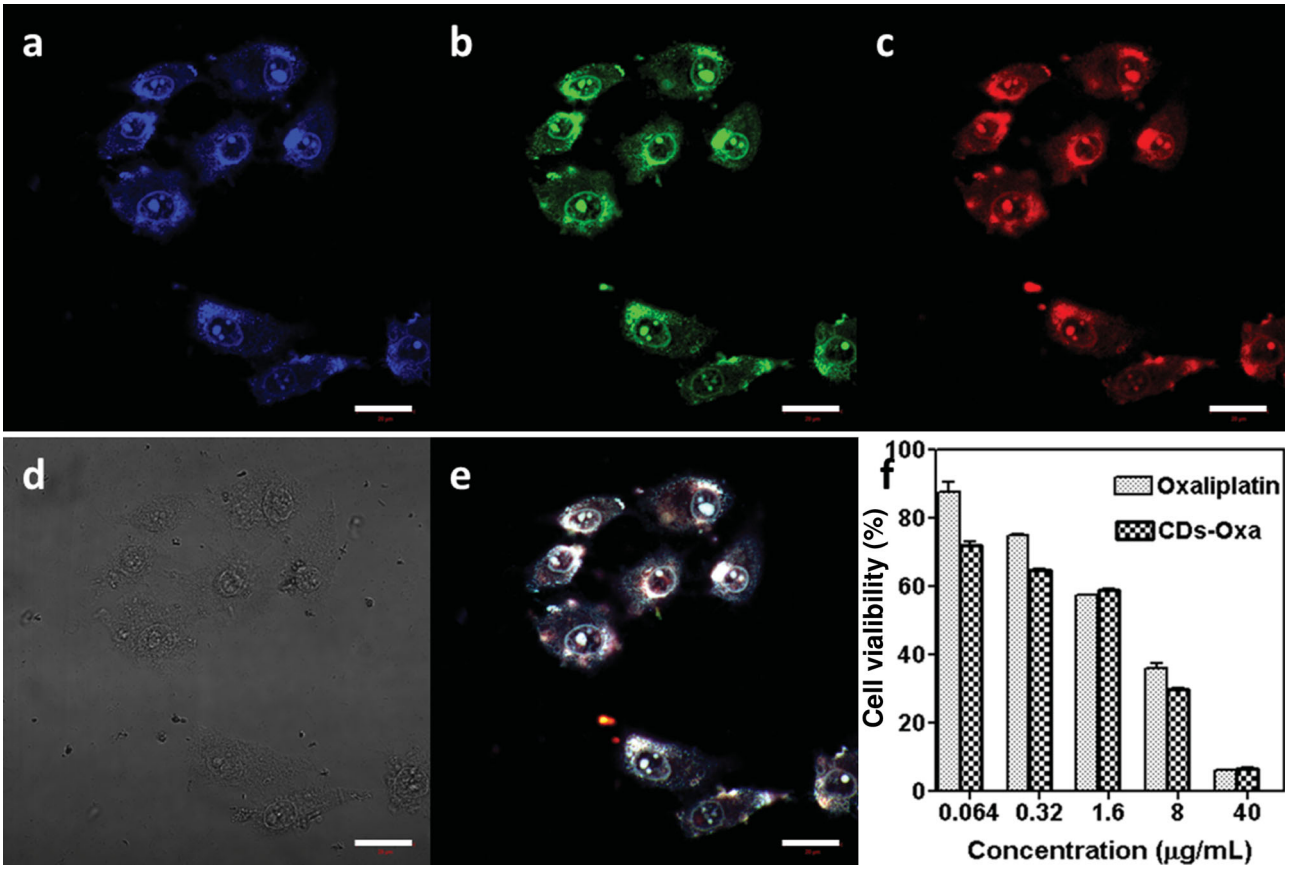

Figure 3. a–d) Confocal fluorescence images of HeLa cells treated with CD-Oxa and imaged under 405 nm (a), 488 nm (b), 555 nm (c) excitation and bright field (d). e) Overlay image of (b–d). The scale bars correspond to 20 μm. f) Cell viability of HepG2 human cancer cells after incubation with oxaliplatin(II) or CD-Oxa for 48 h, determined by MTT assay.

be excited at other wavelengths, for example by green or yellow light, since carbon dots are an excitation-dependent imaging agent. Here, we used blue light as the excitation light source for a short collection time and high signal-to-noise ratio. As shown in **Figure 4**, fluorescence emission from the intralesionally injected CD-Oxa could be readily detected. At the initial injection time, CD-Oxa was concentrated at the injection site and formed a highlight point (Figure 4b), and then the fluorescent area spread around the injection point to form a gradient intensity distribution centered at the tumor site (Figure 4c). Later, such a gradient intensity distribution remained but the intensity decreased gradually with time (Figure 4d), indicating digestion of CD-Oxa particles within the body. After 24 hours, the fluorescence signal had become relatively weak. The second injection was performed, and the fluorescent intensity increased immediately. The fluorescence signal faded gradually over 48 h; a weak fluorescence signal was still observed, implying some of CDs-Oxa remained at the tumor site. At 72 hours after injection, the fluorescence signal had faded almost completely. Figure 4i–m shows optical images of the tumor site after local injection. At the initial injection, there is a protuberance at the tumor site. With increasing time the tumor area tended to become flat, and most of the tumor tissue was necrotic after 72 h treatment with two injections. That implied that CD-Oxa particles had entered the tumor cells and the Pt(IV) had been reduced to the corresponding Pt(II) species with antitumor function as a result of the reducing environment in the cancer cells.[19] This helps lower the toxicity of CD-Oxa towards the normal cells. Figure 4n shows that the tumor size decreased monotonically with the time of therapy; the tumor volume decreased from initially 6.5 cm^3 to 1.2 cm^3 (Figure 4m), which means 82.4% of the tumor was cured within three days. During the whole cure process, we can track the drug in the tumor by virtue of the fluorescence of CDs and realize "personalized medicine", which can be tailored to the individual patient. Another example of individual treatment is shown in Figures S13–S17 in the Supporting Information. A scab was observed within 24 h of injection because the tumor tissue was killed by the theranostic agent CD-Oxa (Figure S14). After 6 days, detachment was observed at the edge of the scab, indicating the growth of new tissue. Figure S15 displays the enhanced fluorescence signal after intralesional injection, which then gradually faded out. Figure S16 shows that the tumor size decreased with the time of therapy; the tumor volume decreased from initially 535.2 mm^3 to 46.6 mm^3, which means 91.3% of the tumor was cured within 6 days. The tumor growth tendency obviously halted afterward. These results confirm that CD-Oxa is very efficacious in killing tumor cells. As shown in Figure S17, body weight decreased slightly in the first three days, and then was well maintained and even increased during subsequent

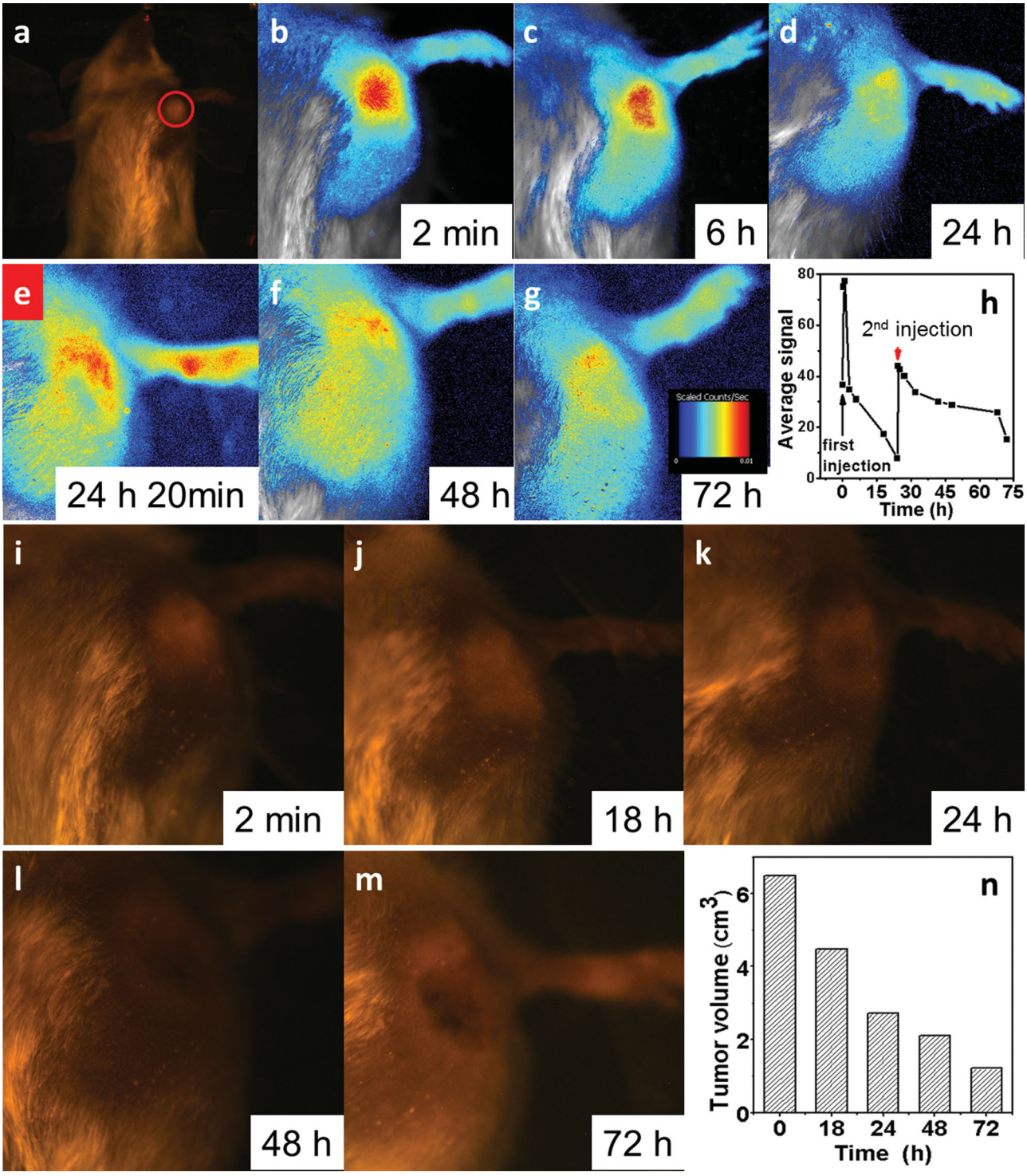

Figure 4. In vivo fluorescence images of mouse bearing H22 liver cancer after the first intralesional injection of CD-Oxa. a) 0 min (taken under white light; the red circle marks the position of tumor), b) 2 min, c) 6 h, d) 24 h, e) 24 h 20 min (the second injection), f) 48 h and g) 72 h. All taken under blue light unless otherwise stated. h) Semiquantitative fluorescence intensities of the tumor area determined at different times. Red arrow indicates the 2nd injection. i–m) Photographs of the tumor area after intralesional injection of CD-Oxa after 2 min (i), 18 h (j), 24 h (k), 48 h (l), and 72 h (m). n) Tumor sizes of H22 xenograft model as a function of time.

treatments, indicating that this kind of theranostic agent had lower toxicity. From the above results and analysis of both the tumor inhibition rate and the systemic toxicity reflected by body weight change, it can be inferred that CD-Oxa is a very effective and reasonable drug that could have potential applications in theranostics.

In summary, a multifunctional theranostic agent (CD-Oxa) was prepared by the conjugation of an anticancer agent (oxidized oxaliplatin, Oxa(IV)-COOH) on the surface of CDs. CD-Oxa successfully integrates the optical properties of CDs and the therapy performance of Oxa. The in vitro results indicate that CD-Oxa possesses good biocompatibility, bioimaging function, and anticancer effect. The in vivo results demonstrate that we can follow the track or distribution of the drug by monitoring the fluorescence signal of CD-Oxa, which helps customize the injection time and dosage of the medicine. We believe that the development of highly biocompatible and fluorescent drug delivery systems based on fluorescent CDs holds great promise for specific drug delivery with minimal side effects and toxicity in cancer patients.

Supporting Information

Supporting Information is available from the Wiley Online Library or from the author.

Acknowledgements

This project was supported by the Open Research Fund of the State Key Laboratory of Polymer Physics and Chemistry. Financial support from the National Natural Science Foundation of China (No. 91227118, 21201159 and 61176016), the Science and Technology Department of Jilin Province (No. 20121801), and the Ministry of Science is gratefully acknowledged. Z.S. appreciates the support of the "Hundred Talent Program" of CAS, and Innovation and Entrepreneurship Program of Jilin. Z.X. acknowledges the support of CIAC start-up fund.

Received: December 19, 2013
Revised: January 22, 2014
Published online: March 14, 2014

[1] a) Z. Cheng, A. Al Zaki, J. Z. Hui, V. R. Muzykantov, A. Tsourkas, *Science* **2012**, *338*, 903; b) P. Rai, S. Mallidi, X. Zheng, R. Rahmanzadeh, Y. Mir, S. Elrington, A. Khurshid, T. Hasan, *Adv. Drug Delivery Rev.* **2010**, *62*, 1094; c) L.-S. Wang, M.-C. Chuang, J. A. Ho, *Int. J. Nanomedicine* **2012**, *7*, 4679; d) M. P. Melancon, M. Zhou, C. Li, *Acc. Chem. Res.* **2011**, *44*, 947; e) K. K. Ng, J. F. Lovell, G. Zheng, *Acc. Chem. Res.* **2011**, *44*, 1105.
[2] P. Huang, J. Lin, X. Wang, Z. Wang, C. Zhang, M. He, K. Wang, F. Chen, Z. Li, G. Shen, D. Cui, X. Chen, *Adv. Mater.* **2012**, *24*, 5104.
[3] J. Xie, S. Lee, X. Chen, *Adv. Drug Delivery Rev.* **2010**, *62*, 1064.
[4] J. Xie, G. Liu, H. S. Eden, H. Ai, X. Chen, *Acc. Chem. Res.* **2011**, *44*, 883.
[5] a) D. Ho, X. Sun, S. Sun, *Acc. Chem. Res.* **2011**, *44*, 875; b) J. Xie, J. Huang, X. Li, S. Sun, X. Chen, *Curr. Med. Chem.* **2009**, *16*, 1278.
[6] a) J.-H. Park, G. von Maltzahn, E. Ruoslahti, S. N. Bhatia, M. J. Sailor, *Angew. Chem. Int. Ed.* **2008**, *47*, 7284; b) V. Bagalkot, L. Zhang, E. Levy-Nissenbaum, S. Jon, P. W. Kantoff, R. Langer, O. C. Farokhzad, *Nano Lett.* **2007**, *7*, 3065; c) M. V. Yezhelyev, L. Qi, R. M. O'Regan, S. Nie, X. Gao, *J. Am. Chem. Soc.* **2008**, *130*, 9006; d) X. Liu, M. Zheng, X. Kong, Y. Zhang, Q. Zeng, Z. Sun, W. J. Buma, H. Zhang, *Chem. Commun.* **2013**, *49*, 3224.
[7] a) N. L. Rosi, D. A. Giljohann, C. S. Thaxton, A. K. R. Lytton-Jean, M. S. Han, C. A. Mirkin, *Science* **2006**, *312*, 1027; b) J. D. Gibson, B. P. Khanal, E. R. Zubarev, *J. Am. Chem. Soc.* **2007**, *129*, 11653; c) M. Prabaharan, J. J. Grailer, S. Pilla, D. A. Steeber, S. Gong, *Biomaterials* **2009**, *30*, 6065.
[8] N. W. S. Kam, Z. Liu, H. Dai, *Angew. Chem. Int. Ed.* **2006**, *45*, 577.
[9] J. E. Lee, N. Lee, T. Kim, J. Kim, T. Hyeon, *Acc. Chem. Res.* **2011**, *44*, 893.
[10] H. Kobayashi, M. Ogawa, R. Alford, P. L. Choyke, Y. Urano, *Chem. Rev.* **2009**, *110*, 2620.
[11] a) S. Achilefu, *Chem. Rev.* **2010**, *110*, 2575; b) M. Green, *Angew. Chem. Int. Ed.* **2004**, *43*, 4129.
[12] S. N. Baker, G. A. Baker, *Angew. Chem. Int. Ed.* **2010**, *49*, 6726.
[13] a) H. Li, Z. Kang, Y. Liu, S.-T. Lee, *J. Mater. Chem.* **2012**, *22*, 24230; b) H. Li, X. He, Z. Kang, H. Huang, Y. Liu, J. Liu, S. Lian, C. H. A. Tsang, X. Yang, S.-T. Lee, *Angew. Chem. Int. Ed.* **2010**, *49*, 4430.
[14] a) L. Li, G. Wu, G. Yang, J. Peng, J. Zhao, J.-J. Zhu, *Nanoscale* **2013**, *5*, 4015; b) L. Cao, M. J. Meziani, S. Sahu, Y.-P. Sun, *Acc. Chem. Res.* **2012**, *46*, 171.
[15] L. Wu, M. Luderer, X. Yang, C. Swain, H. Zhang, K. Nelson, A. J. Stacy, B. Shen, G. M. Lanza, D. Pan, *Theranostics* **2013**, *3*, 677.
[16] J. Tang, B. Kong, H. Wu, M. Xu, Y. Wang, Y. Wang, D. Zhao, G. Zheng, *Adv. Mater.* **2013**, *25*, 6569.
[17] B. Rosenberg, L. Vancamp, J. E. Trosko, V. H. Mansour, *Nature* **1969**, *222*, 385.
[18] T. Alcindor, N. Beauger, *Curr. Oncol.* **2011** ,*18* ,18.
[19] H. Xiao, W. Li, R. Qi, L. Yan, R. Wang, S. Liu, Y. Zheng, Z. Xie, Y. Huang, X. Jing, *J. Controlled Release* **2012**, *163*, 304.
[20] a) M. Zheng, Z. Xie, D. Qu, D. Li, P. Du, X. Jing, Z. Sun, *ACS Appl. Mater. Interfaces* **2013**, *5*, 13242; b) D. Qu, M. Zheng, P. Du, Y. Zhou, L. Zhang, D. Li, H. Tan, Z. Zhao, Z. Xie, Z. Sun, *Nanoscale* **2013**, *5*, 12272.
[21] a) M. Li, N. Tang, W. Ren, H. Cheng, W. Wu, W. Zhong, Y. Du, *Appl. Phys. Lett.* **2012**, *100*, 233112; b) D. Wei, Y. Liu, Y. Wang, H. Zhang, L. Huang, G. Yu, *Nano Lett.* **2009**, *9*, 1752.
[22] S. Zhu, J. Zhang, S. Tang, C. Qiao, L. Wang, H. Wang, X. Liu, B. Li, Y. Li, W. Yu, X. Wang, H. Sun, B. Yang, *Adv. Funct. Mater.* **2012**, *22*, 4732.
[23] H. Xiao, H. Song, Y. Zhang, R. Qi, R. Wang, Z. Xie, Y. Huang, Y. Li, Y. Wu, X. Jing, *Biomaterials* **2012**, *33*, 8657.
[24] F. Celikoglu, S. I. Celikoglu, E. P. Goldberg, *Cancer Ther.* **2008**, *6*, 545.